Correspondence to:
M. K. Brown,
m.brown.12@bham.ac.uk

Future Climate Change in the Thermosphere Under Varying Solar Activity Conditions

M. K. Brown[1,2] [iD], **H. G. Lewis[2]** [iD], **A. J. Kavanagh[3]** [iD], **I. Cnossen[3]** [iD], and **S. Elvidge[1]** [iD]

[1]Space Environment and Radio Engineering Group (SERENE), University of Birmingham, Birmingham, UK, [2]University of Southampton, Southampton, UK, [3]British Antarctic Survey, Cambridge, UK

Abstract Increasing carbon dioxide concentrations in the mesosphere and lower thermosphere are increasing radiative cooling in the upper atmosphere, leading to thermospheric contraction and decreased neutral mass densities at fixed altitudes. Previous studies of the historic neutral density trend have shown a dependence upon solar activity, with larger F10.7 values resulting in lower neutral density reductions. To investigate the impact on the future thermosphere, the Whole Atmosphere Community Climate Model with ionosphere and thermosphere extension has been used to simulate the thermosphere under increasing carbon dioxide concentrations and varying solar activity conditions. These neutral density reductions have then been mapped onto the Shared Socioeconomic Pathways published by the Intergovernmental Panel on Climate Change. The neutral density reductions can also be used as a scaling factor, allowing commonly used empirical models to account for CO_2 trends. Under the "best case" SSP1-2.6 scenario, neutral densities reductions at 400 km altitude peak (when $CO_2 = 474$ ppm) at a reduction of 13%–30% (under high and low solar activity respectively) compared to the year 2000. Higher CO_2 concentrations lead to greater density reductions, with the largest modeled concentration of 890 ppm resulting in a 50%–77% reduction at 400 km, under high and low solar activity respectively.

Plain Language Summary Carbon dioxide (CO_2) concentrations are increasing throughout the atmosphere, not just at ground level. While this results in global warming in the lower atmosphere, the much less dense upper atmosphere does not trap the radiated heat, resulting in cooling of the upper atmosphere. As the upper atmosphere cools, it contracts, reducing the atmospheric density at a fixed altitude. Satellites traveling in low Earth orbit, such as the International Space Station at 400 km altitude, experience atmospheric drag, slowly reducing their altitude until they "re-enter" and burn up in the lower, denser atmosphere. Reducing neutral densities will increase satellite orbital lifetimes as they experience less drag. The upper atmosphere has been simulated under increasing CO_2 concentrations and solar activity conditions. This has also been linked to potential future CO_2 concentration scenarios. Scaling factors have been created allowing simpler, faster models to account for CO_2 density reductions. Under a best-case scenario (SSP1-2.6) where CO_2 concentrations peak in around the year 2065 and then decline, densities at 400 km are 13%–30% lower compared to the year 2000 at the CO_2 peak concentration, and then recover as CO_2 reduces. However, densities continue to reduce if CO_2 concentrations keep rising.

1. Introduction

Carbon dioxide (CO_2) exists throughout the atmosphere (shown in Figure 1) (Yue et al., 2015) with a roughly constant concentration in the turbulent atmosphere below the homopause (around 90 km altitude). Gravitational separation asymptotically decreases the concentration with altitude trending toward zero in the lower thermosphere (around 200 km).

Carbon dioxide can gain energy via collisions with molecules or ions in the atmosphere, or absorbing infra-red (IR) radiation. It can then lose that energy via collisions, or emission of IR radiation (at 15 μm). In the dense lower atmosphere, collisions dominate, and any emitted IR radiation has a short mean free path, being quickly recaptured and trapping heat locally, leading to the greenhouse effect. In the less-dense upper atmosphere, collisions are much less frequent, so CO_2 is more likely to lose energy via IR emission, which has a much longer mean free path, allowing heat to escape the locale, cooling the upper atmosphere. As the upper atmosphere cools, it contracts, resulting in the neutral density reducing at a given fixed altitude.
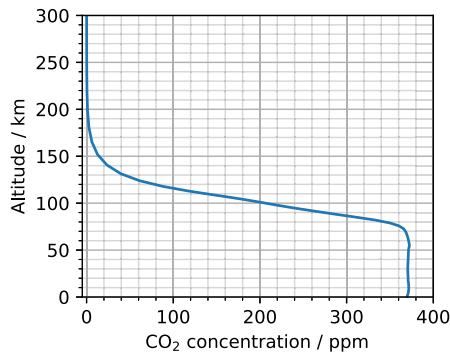
Figure 1. Altitude profile of carbon dioxide concentration, from ground level through to the lower thermosphere. This example is a global average of Whole Atmosphere Community Climate Model with ionosphere and thermosphere extension output for the year 2000.

Similarly to CO_2, Nitric oxide (NO) also cools the upper atmosphere with IR emission at 5.3 μm. Concentrations of NO, and also atomic oxygen (O), vary with solar activity levels (Mlynczak et al., 2014). This changes the ratio of NO to CO_2, as well as the temperature and collision rates with O, such that the magnitude of neutral density reductions in the upper atmosphere is dependent on solar activity. The largest reductions are seen under low solar activity, when CO_2 is relatively more important for the thermosphere's energy budget. The large amount of molecular nitrogen (N_2) in the lower atmosphere acts as a reservoir, such that additional nitrogen dioxide (NO_2) released as a greenhouse gas is assumed to have minimal impact on NO concentrations.

A large number of previous studies have both modeled and observed the reducing density trend first predicted by Roble and Dickinson (1989). Observed neutral density reductions are summarized in Table 1, modeled values in Table 2, and Figure 2 shows the altitude profile of both observed and modeled reductions in literature. All values have been standardized to a density trend given in "% per decade." While the magnitude of the reductions vary across the literature, all studies agree on a reducing density trend within the upper atmosphere. The studies that also binned density trends by solar activity agreed that the trend is larger in magnitude under low solar activity.

These secular trends in neutral density have an impact on the space debris environment in low Earth orbit (LEO), reducing atmospheric drag acting on orbiting objects and increasing their orbital lifetimes (Lewis et al., 2011). Models of the space debris environment make use of computationally fast empirical atmospheric models to propagate orbits while accounting for atmospheric drag, however these empirical atmospheric models do not account for secular CO_2 trends. The aims of this study are therefore twofold. First to build upon the future neutral density reductions under low solar activity results of Brown et al. (2021), by understanding how the magnitude of the density reduction varies with increasing solar activity and CO_2 concentration. Second to provide scaling factors which allow empirical atmospheric models to account for long-term trends caused by CO_2 emissions. These scaling factors maintain the speed and ease-to-run advantages of empirical models over numerical models,

Table 1
Summary of Observed (Derived) Neutral Density Trends at 400 km Altitude

| Study	Model used	F10.7 (sfu)	Period	Density trend (% per decade)
Keating et al. (2000)[a]	MET99	~75	1976, 1986, 1996	−4.9 ± 1.3
Emmert et al. (2004)	NRLMSISE-00	≤90	1996–2001	−3.8
Emmert et al. (2004)	NRLMSISE-00	All	1996–2001	−2.8 ± 1.0
Marcos et al. (2005)	NRLMSISE-00	All	1970–2000	−1.7 ± 0.2
Emmert et al. (2008)	GAMDM	<75	1967–2007	−5.5 ± 1.4
Emmert et al. (2008)	GAMDM	170 to 220	1967–2007	−2.1 ± 0.9
Saunders et al. (2011)	NRLMSISE-00	<90	1970–2010	−7.2
Saunders et al. (2011)	NRLMSISE-00	All	1970–2010	−5.4 ± 3
Saunders et al. (2011)	NRLMSISE-00	>90	1970–2010	−4.0
Emmert and Picone (2011)	GAMDM	All	1967–2005	−1.94 ± 0.68
Emmert (2015)	GAMDM2.1	60 to 75	1967–2005	−3.1 ± 1.6
Emmert (2015)	GAMDM2.1	60 to 75	1967–2013	−7.2 ± 1.2
Emmert (2015)	GAMDM2.1	180 to 500	1967–2005	−3.0 ± 0.7
Emmert (2015)	GAMDM2.1	180 to 500	1967–2013	−3.0 ± 0.8
Weng et al. (2020)	ANNM	All	1967–2013	−1.7

Note. "Model used" refers to the atmospheric model used to remove the dominant solar cycle variation, and detrend the data.
[a] 350 km altitude.

Table 2
Summary of the Modeled Historic Neutral Density Trends at 400 km Altitude

Study	Model used	F10.7 (sfu)	Period	Density trend (% per decade)
Qian et al. (2006)	TIME-GCM (1D)	70	1970–2000	−2.5[a]
Qian et al. (2006)[b]	TIME-GCM (1D)	All	1970–2000	−1.7
Qian et al. (2006)	TIME-GCM (1D)	210	1970–2000	−0.75[a]
Solomon et al. (2015)	TIME-GCM	70	1996–2008	−4.9 or −6.8[c]
Solomon et al. (2015)	TIME-GCM	200	1996–2008	−1.8 or −2.1[c]
Solomon et al. (2018)	WACCM-X	70	1974–2003	−3.9
Solomon et al. (2019)	WACCM-X	200	1974–2003	−1.7
Cnossen (2020)	WACCM-X 2.0	All	1950–2015	−2.8 ± 0.6
Brown et al. (2021)	WACCM-X	70	1975–2005	−5.8

[a]Average of the 350 and 450 km values. [b]Result was re-presented by Qian and Solomon (2011). [c]k_q, CO_2-O collisional deactivation rate, of 1.5×10^{-12} or 3.0×10^{-12} cm^3 s^{-1}.
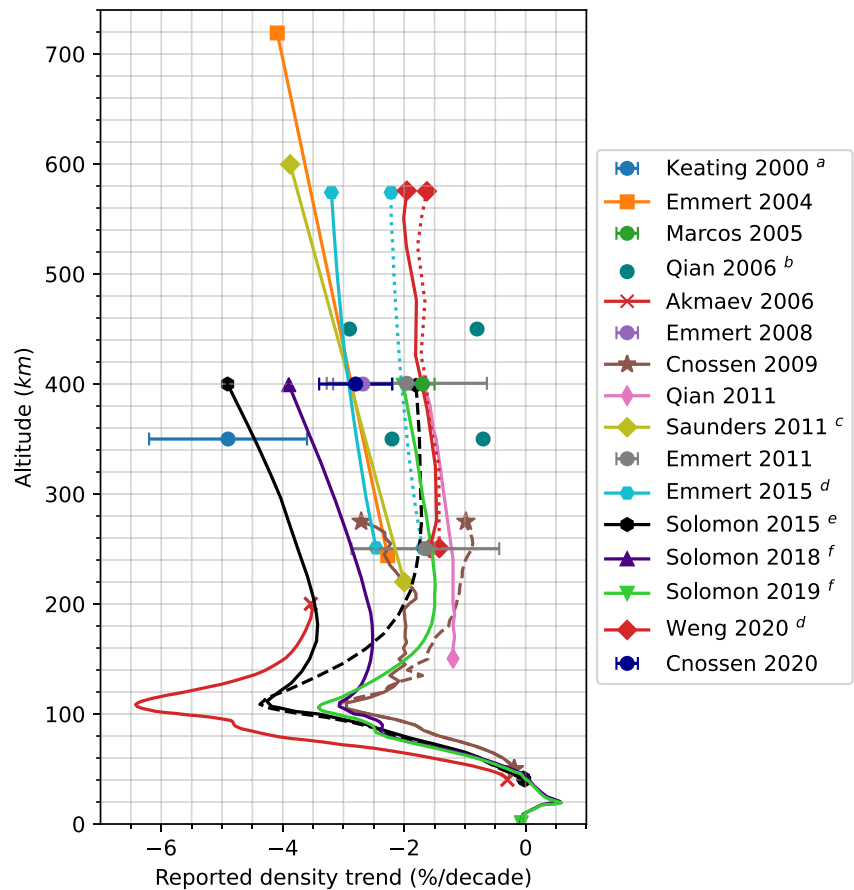
Figure 2. Summary of historical density trends at 400 km in the literature for varying solar activity levels, with detail on values used given in Tables 1 and 2. Error bars are provided where available. Updated version of similar figures in Emmert et al. (2008) and Solomon et al. (2015). [a] Keating et al. (2000) value at 350 km. [b] Plotted line is mean of 350 and 450 km trends in Qian et al. (2006). [c] Saunders et al. (2011) used large binning for F10.7, so the lines denote trends found for F10.7 less than or greater than 90 sfu. [d] Emmert (2015) and Weng et al. (2020) calculated the trend over different periods. The solid line denotes 1967 to 2005 and the dotted line denotes 1967 to 2013. [e] CO_2–O quenching rate, k_q, affects the CO_2 cooling rate and therefore the magnitude of trend. Solomon et al. (2015) used the default k_q of the model, 1.5×10^{-12} (solid line), and also 3.0×10^{-12} (dashed line). [f] Solomon et al. (2018, 2019) use the same methodology, but at low and high solar activity values respectively.

while allowing for CO_2 induced trends to be included in orbital lifetime estimation and debris environment modeling.

2. Model

The Whole Atmosphere Community Climate Model with thermosphere and ionosphere extension (WACCM-X) was used to model the thermospheric response to increasing levels of CO_2, with the model fully described by Liu et al. (2010). The model is part of the Community Earth System Model (CESM) (Hurrell et al., 2013), maintained by the National Center for Atmospheric Research. Version 1.2.2 of the model was used rather than the newer 2.0 (Liu et al., 2018) to build upon the reprocessed results of Brown et al. (2021) and allow for direct comparison. As a whole atmosphere numerical model, WACCM-X solves for the physics, chemistry and dynamics of the atmosphere, starting from some initial state and moving forwards in time. This allows ground-level CO_2 to propagate upwards to the thermosphere. A 1.9 by 2.5° latitude by longitude grid with quarter scale height vertical resolution was used up to a maximum model height of 4×10^{-10} hPa. This top level of the model varies in altitude between around 350 to 600 km depending upon energy input.

3. Methodology

WACCM-X has been used to simulate the whole atmosphere under different, fixed carbon dioxide concentrations, under low and high solar activity conditions, as well as varying solar activity conditions at one fixed, high CO_2 concentration. As a numerical model, WACCM-X requires a spin-up time for the model to move from its initial conditions toward a steady state more representative of the input conditions. A sudden, large increase in ground-level CO_2 takes a substantial amount of time to propagate through to the upper atmosphere. To speed up the spin-up process, the CO_2 profile in the initial state of the year 2000 (Figure 1) is scaled by the relative increase in ground-level CO_2 concentration. Above 60 km, photodissociation breaks CO_2 into carbon monoxide (CO) and O, which can then reform, such that CO_2 and CO exist in chemical equilibrium in the thermosphere. Therefore the CO profile is scaled similarly to CO_2. After this scaling, WACCM-X has 4 months of spin-up before data is used for analysis. This allows for a steady state to be reached, for example, by allowing the scaled CO_2 and CO concentrations to reach a chemical equilibrium via WACCM-X chemical reactions at the currently modeled solar activity level.

Geomagnetic activity was held at a Kp value of 0 throughout the simulations to remove geomagnetic activity effects, and to match results with Brown et al. (2021). It is noted that the most commonly occurring Kp value is 1, and may have been a better choice as the default. However, Emmert (2015) identified no significant difference between these two values in historic observed trends.

With increasing traffic to LEO orbits, there is a strong need to understand the neutral density trends in this region. The US Naval Research Laboratory's Mass Spectrometer and Incoherent Scatter radar model (NRLMSISE-00) (Picone et al., 2002) shows that helium can contribute over 15% of the total, globally averaged neutral density at altitudes higher than around 500 km during low solar activity, but helium is not modeled by WACCM-X. The neutral density extrapolation technique used in Brown et al. (2021) failed to account for helium, so extrapolation and neutral density trends were limited in altitude to 500 km. In this study, a different extrapolation technique which includes helium is used instead (which is also applied to the Brown et al. (2021) results). As helium is chemically inert, it can be added by an uncoupled model (Kim et al., 2012; Sutton et al., 2015). In post-processing, NRLMSISE-00 is used to calculate atomic oxygen and helium number densities under similar solar activity, times, and grid points as the WACCM-X simulations. These NRLMSISE-00 helium profiles are then scaled by the atomic oxygen fractional difference between the NRLMSISE-00 and WACCM-X profiles, as in:

$$He_{WACCM\text{-}X} = \frac{O_{WACCM\text{-}X}}{O_{NRLMSISE\text{-}00}} He_{NRLMSISE\text{-}00} \tag{1}$$

at each grid point. The number density profile of each species is then extrapolated to higher altitudes using Bates-Walker (Walker, 1965) profiles via

$$n(i|z) = n(i|\infty)\exp\left[-\frac{m_i g_{ref}}{kT_\infty}\frac{(z - z_\infty)(R + z_{ref})}{R + z}\right] \tag{2}$$
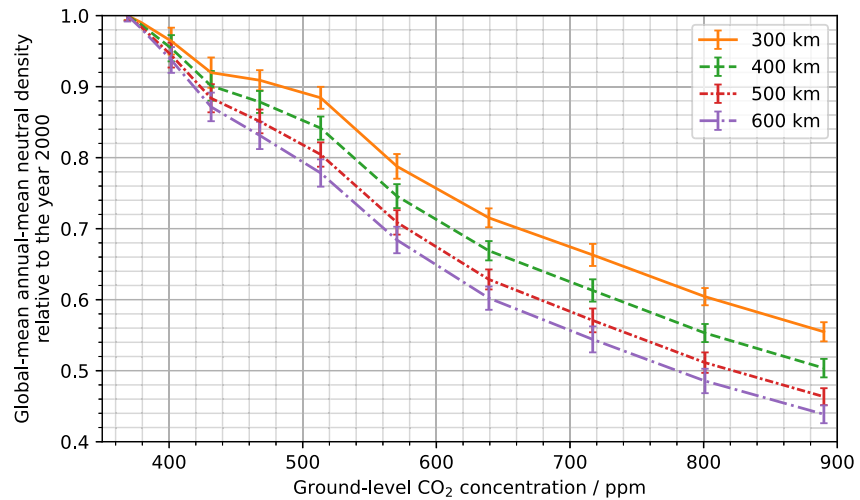
Figure 3. Neutral density reductions relative to the year 2000, at F10.7 of 200 sfu, under increasing ground-level carbon dioxide concentrations. These can be used as scaling factors for an empirical thermospheric model to include CO_2 density reductions, under high solar activity conditions.

where $n(i|z)$ is the number density of constituent i at altitude z, m_i is the mass of the constituent, g_{ref} is the gravity at the reference altitude z_{ref} (taken as the level below the top level of WACCM-X), k is the Boltzmann constant and R is the Earth's radius. T_∞ is the exospheric temperature, which is assumed to be the WACCM-X top level temperature. z_∞ is the altitude at which the exospheric temperature is taken. The number density profiles are converted to mass densities, and neutral mass density is then obtained by summing the O and He profiles.
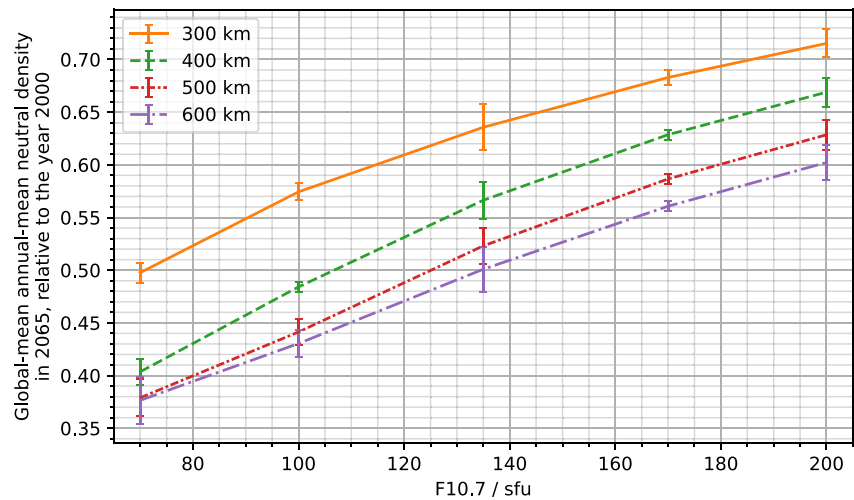
4. High Solar Activity Results

WACCM-X was used to simulate carbon dioxide concentrations which correspond to Representative Concentration Pathway 8.5 (RCP8.5) (Intergovernmental Panel on Climate Change (IPCC), 2014) for a snapshot every 10 years from 2015 to 2095 inclusive, as well as the year 2000 as a reference point. These concentrations were chosen to match (Brown et al., 2021), but 2005 was neglected due to the small change expected with respect to the year 2000. Each of these was run cyclically for 5 years and the global-mean annual-means taken, where 5 years was chosen to better understand the standard deviation between different model realizations. Results are shown in Figure 3. Global-mean annual-means are taken to remove seasonal dependencies.

5. Varying Solar Activity Results

Historic studies, and the above results (compared against the low solar activity results of Brown et al. (2021)), show that neutral density reductions are smaller in magnitude during high solar activity. To understand how the reduction depends on solar activity conditions in more detail, WACCM-X was used to simulate the years 2000 and 2065 (639 ppm) under F10.7 values of 100, 135, and 170 sfu. This provided enough points to outline the relationship (linear vs. nonlinear) with the limited computing resources available. The year 2065 (639 ppm) was chosen as a large enough CO_2 concentration to result in larger neutral density reductions to identify the trend, while being low enough that it appears in most RCP and Shared Socioeconomic Pathway (SSP) scenarios. Each of these was run cyclically for 2 years and the global-mean annual-means taken, where 2 years was chosen due to computing time limitations. Results are shown in Figure 4, along with the equivalent 70 sfu values from the reprocessed results of Brown et al. (2021) using the updated methodology, and 200 sfu of Figure 3.

To combine the low, high and varying solar activity results, Figure 5 uses 2D cubic interpolation on each altitude shell to obtain the F10.7-CO_2 combinations which were not simulated with WACCM-X. This inherently assumes the relationship shown in Figure 4 maps to other CO_2 concentrations, and is scaled to the lower and upper limits of the low and high solar activity runs. This provides scaling factors relative to the year 2000, dependent upon solar activity (70–200 sfu), altitude (200–1,000 km), and CO_2 concentrations (around 370–890 ppm).
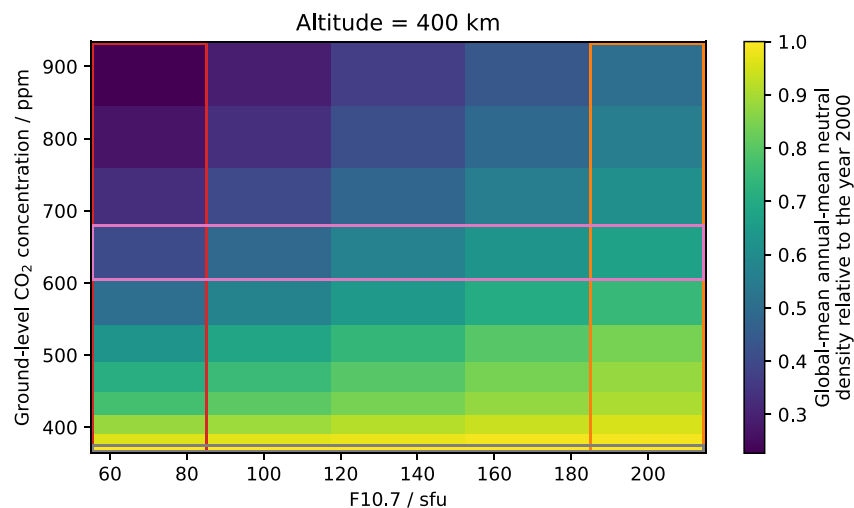
Figure 4. Neutral density reductions relative to the year 2000, at a CO_2 concentration of 639 ppm, under varying solar activity conditions.

6. Discussion

In both the low solar activity results of Brown et al. (2021) and the high solar activity results of Figure 3, there is a sudden decrease in the rate at which neutral densities reduce between CO_2 concentrations of around 440 and 520 ppm, which then recovers by 550 ppm. This does not correlate with any of the input parameters to WACCM-X, so it cannot be readily attributed to it being an artifact of the model itself, a combination of input parameters, or an unidentified physical phenomenon.

While the historic trends summarized in Figure 2 often present results in units of "% per decade," this inherently includes the historic increase in carbon dioxide during the period the trend is calculated over. Extrapolating "% per decade" trends forward assumes the rate of increase in CO_2 concentrations will remain constant. Figure 6 and Table 3 show the observed trends of Table 1 mapped into carbon dioxide concentration-based trends, with the year 2000 (CO_2 = 369 ppm) taken as the reference point. This was done by assuming the stated trends are fixed over each study's period, calculating the scaled neutral densities at the start and end of the period, then by assuming the density reduction for each ppm drop in carbon dioxide concentration is consistent, this percentage change in

Figure 5. Neutral density reductions (scaling factors) at 400 km altitude. Bins outlined in red indicate low F10.7 runs at 70 sfu (reprocessed from Brown et al. (2021)), orange are high F10.7 (200 sfu of Figure 3), pink are varying F10.7 runs at a fixed 639 ppm (shown in Figure 4), and gray is the reference line (year 2000) where all ratios equal 1. Other bins are obtained by 2D cubic interpolation.
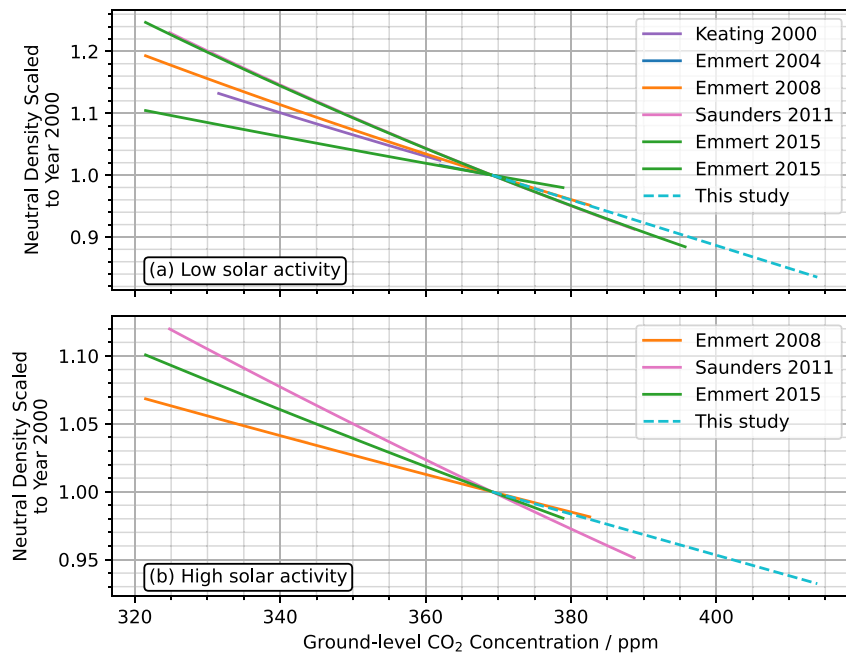
Figure 6. Historic density trends at 400 km of Table 1 mapped into CO_2 concentrations and taking the year 2000 as a reference point, along with the 2000 to 2020 density reductions modeled in this study. Subfigures show low and high solar activity conditions. Emmert (2015) appears twice as the trend was calculated over two different periods.

neutral density per CO_2 ppm can be calculated. Providing trends in units of "%/ppm" allows for validation through direct comparison with the density reduction results from the period 2000–2020 of this study. The low solar activity results are the middle of the range of historic observed trends. The high solar activity trend is smaller in magnitude within the range of these studies. Observed trends in Table 1 calculated over all solar activity levels were neglected as they did not match to the fixed solar activity levels used in the WACCM-X simulations.

Table 3
Summary of Observed (Derived) Neutral Density Trends at 400 km Altitude Under Low and High Solar Activity Levels, Converted to Trends Stated in Carbon Dioxide Concentration (%/ppm)

Study	Solar activity	Period	%/ppm
Keating et al. (2000)	Low	1976–1996	−0.329
Emmert et al. (2004)	Low	1996–2001	−0.223
Emmert et al. (2008)	Low	1967–2007	−0.370
Saunders et al. (2011)	Low	1970–2010	−0.466
Emmert (2015)	Low	1967–2005	−0.208
Emmert (2015)	Low	1967–2013	−0.462
This study	Low	2000–2020	−0.402
Emmert et al. (2008)	High	1967–2007	−0.139
Saunders et al. (2011)	High	1970–2010	−0.255
Emmert (2015)	High	1967–2005	−0.201
This study	High	2000–2020	−0.157

Note. Period has been included to highlight if the trend was calculated through the 2008 solar minimum.

Recent trends calculated through the solar minima of 2008 and 2020 have had to contend with the uncommonly low solar activity of these solar minima years, during which the empirical thermospheric models used to remove solar variability before trend calculation over-predict neutral densities. This changes calculated long-term trends, as demonstrated by Emmert (2015) and their two trends calculated over different periods, as summarized in Table 1. This phenomenon convoluted validation through comparison of the scaled neutral densities of empirical models with accelerometer-derived densities from satellites such as the Gravity Recovery and Climate Experiment (Siemes et al., 2023), and the TLE-derived densities of Emmert (2015).

The Intergovernmental Panel on Climate Change (IPCC) has published the Shared Socioeconomic Pathways (SSPs) which contain future possible CO_2 concentrations (Lee et al., 2023). These reduce the extensive possibilities in the literature to a limited number of scenarios which can be commonly used between studies. Four of the SSPs (SSP1-2.6, SSP2-4.5, SSP3-7.0, and SSP5-8.5), shown in Figure 7, represent a subset of the SSPs which range across the possible CO_2 concentration projections, while also being similar to the older RCPs. For additional context, SSP1-2.6 represents a "best-case" scenario where the CO_2 concentration peaks at 474 ppm around the year 2065, and then begins to reduce as carbon capture technologies remove more CO_2 than is emitted. In contrast, SSP5-8.5 represents a "worst-case" scenario where this is continued and accelerating CO_2 emissions through increasing fossil fuel usage. SSP2-4.5 and SSP3-7.0 are then chosen to represent middle CO_2
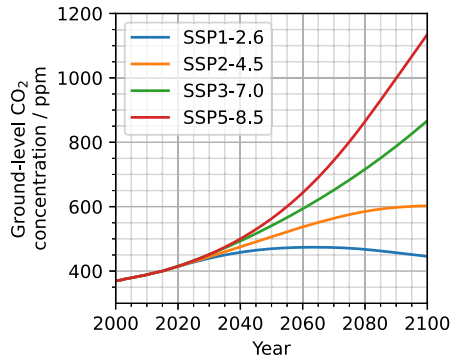
Figure 7. Future carbon dioxide concentration taken from four of the Shared Socioeconomic Pathways (SSPs) published by the Intergovernmental Panel on Climate Change (Lee et al., 2023).

concentration projections between the two extremes, representing "middle-of-the-road" and "minimal adaptation" scenarios respectively.

The F10.7 and CO_2 dependence of the neutral density reductions at 400 km are shown in Figure 5. By assuming an empirical model gives a true representation of the year 2000, these neutral density reductions can be used as scaling factors. The neutral densities output by an empirical model (i.e., NRLMSISE-00) can be multiplied by the scaling factors to account for the CO_2 induced neutral density reductions. The scaling factors (neutral density reductions) can then also be mapped to each SSP's future CO_2 concentrations, as shown in Figure 8. These scaling factors are included in the published data, with altitude, F10.7 and CO_2 dependence, or mapped to the SSPs so only the future F10.7 dependence needs to be specified. This allows empirical models to be used for long-term orbital propagation or debris environment modeling while accounting for thermospheric CO_2 trends and maintaining the computation speed of empirical models required for these applications.

Solar activity has a substantial impact on neutral density reductions, but solar activity forecasts on the order of years to decades are notoriously difficult (Nandy, 2021). To demonstrate the solar activity impact, solar cycles 23 and 24 are repeated in Figure 8. These density reductions are applied in addition to the order-of-magnitude change in neutral density caused by solar activity, and can be applied to output from empirical models (by assuming that model is an accurate representation of the year 2000). In the SSP1-2.6 scenario, as CO_2 concentrations peak and decline, neutral densities begin to recover. However, looking at this "best-case" scenario, the reduced neutral densities are between 13% and 30% lower during the peak CO_2 period, which will substantially increase orbital lifetimes. In general, this will increase the likelihood of collision during an object's lifetime, creating more fragments, which further increases the likelihood of collision in a feedback loop. This is being investigated in further work.

7. Conclusions

WACCM-X has been used to simulate the thermospheric response and contraction to increasing CO_2 concentrations under varying solar activity conditions. In general, the neutral density reductions increase in magnitude with altitude, increase with carbon dioxide concentration, and decrease with solar activity (F10.7). Through use of
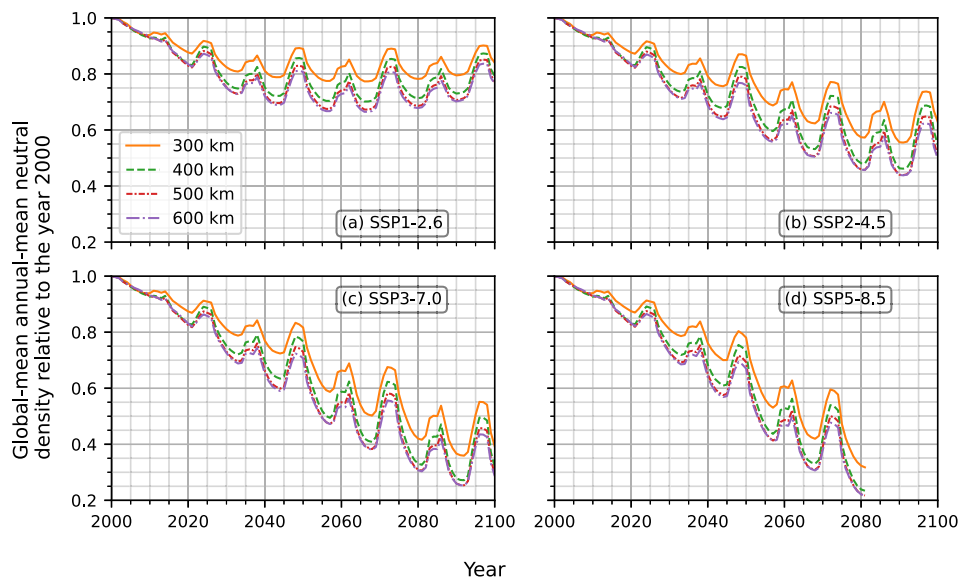
Figure 8. Density reductions (scaling factors) under the four Shared Socioeconomic Pathways (SSPs) shown in Figure 7. Solar cycles 23 and 24 are repeated into the future to demonstrate the impact of solar activity. Subfigure (d), showing SSP5-8.5, ends in 2080 as higher CO_2 values were not modeled.

the CO_2 concentration scenarios from the SSPs, neutral density reductions (scaling factors) can be mapped onto future years. These scaling factors are being made available as a method of including carbon dioxide-induced neutral density reductions in empirical models, as a much faster solution compared to numerical models. This requires assuming the empirical model, is an accurate representation of the year 2000. However, this opens up including long-term trends into applications such as orbital propagation, lifetime estimation, or space debris environment evolution, and without the need to fully replace the currently used atmospheric models.

Data Availability Statement

The authors acknowledge the contributions of those who helped develop CESM and WACCM-X. These models are publicly available from http://www.cesm.ucar.edu/models/. The data produced and processed for this study is available at: https://doi.org/10.5285/09198c58032d4b8197fd7c6748b92785.

The scaling factors allowing empirical models to account for CO_2 reductions are available at: https://doi.org/10.25500/edata.bham.00001075.

References

Brown, M. K., Lewis, H. G., Kavanagh, A. J., & Cnossen, I. (2021). Future decreases in thermospheric neutral density in low Earth orbit due to carbon dioxide emissions. *Journal of Geophysical Research: Atmospheres*, *126*(8), 1–11. https://doi.org/10.1029/2021JD034589

Cnossen, I. (2020). Analysis and attribution of climate change in the upper atmosphere from 1950 to 2015 simulated by WACCM-X. *Journal of Geophysical Research: Space Physics*, *125*(12), e2020JA028623. https://doi.org/10.1029/2020JA028623

Emmert, J. T. (2015). Altitude and solar activity dependence of 1967–2005 thermospheric density trends derived from orbital drag. *Journal of Geophysical Research: Space Physics*, *120*(4), 2940–2950. https://doi.org/10.1002/2015JA021047

Emmert, J. T., & Picone, J. M. (2011). Statistical uncertainty of 1967–2005 thermospheric density trends derived from orbital drag. *Journal of Geophysical Research*, *116*(A2), A00H09. https://doi.org/10.1029/2010JA016382

Emmert, J. T., Picone, J. M., Lean, J. L., & Knowles, S. H. (2004). Global change in the thermosphere: Compelling evidence of a secular decrease in density. *Journal of Geophysical Research*, *109*(A2), A02301. https://doi.org/10.1029/2003JA010176

Emmert, J. T., Picone, J. M., & Meier, R. R. (2008). Thermospheric global average density trends, 1967–2007, derived from orbits of 5000 near-Earth objects. *Geophysical Research Letters*, *35*(5), L05101. https://doi.org/10.1029/2007GL032809

Hurrell, J. W., Holland, M. M., Gent, P. R., Ghan, S., Kay, J. E., Kushner, P. J., et al. (2013). The Community Earth System Model: A framework for collaborative research. *Bulletin of the American Meteorological Society*, *94*(9), 1339–1360. https://doi.org/10.1175/BAMS-D-12-00121.1

Intergovernmental Panel on Climate Change (IPCC). (2014). *Climate change 2013 – The physical science basis: Working Group I contribution to the fifth assessment report of the Intergovernmental Panel on Climate Change*. Cambridge University Press. https://doi.org/10.1017/CBO9781107415324

Keating, G. M., Tolson, R. H., & Bradford, M. S. (2000). Evidence of long term global decline in the Earth's thermospheric densities apparently related to anthropogenic effects. *Geophysical Research Letters*, *27*(10), 1523–1526. https://doi.org/10.1029/2000GL003771

Kim, J. S., Urbina, J. V., Kane, T. J., & Spencer, D. B. (2012). Improvement of TIE-GCM thermospheric density predictions via incorporation of helium data from NRLMSISE-00. *Journal of Atmospheric and Solar-Terrestrial Physics*, *77*, 19–25. https://doi.org/10.1016/j.jastp.2011.10.018

Lee, H., Calvin, K., Dasgupta, D., Krinmer, G., Mukherji, A., Thorne, P., et al. (2023). *Synthesis report of the IPCC sixth assessment report (AR6), longer report*. IPCC.

Lewis, H. G., Saunders, A., Swinerd, G. G., & Newland, R. J. (2011). Effect of thermospheric contraction on remediation of the near-Earth space debris environment. *Journal of Geophysical Research*, *116*(A2), A00H08. https://doi.org/10.1029/2011JA016482

Liu, H. L., Bardeen, C. G., Foster, B. T., Lauritzen, P., Liu, J., Lu, G., et al. (2018). Development and validation of the Whole Atmosphere Community Climate Model with thermosphere and ionosphere extension (WACCM-X 2.0). *Journal of Advances in Modeling Earth Systems*, *10*(2), 381–402. https://doi.org/10.1002/2017MS001232

Liu, H. L., Foster, B. T., Hagan, M. E., McInerney, J. M., Maute, A., Qian, L., et al. (2010). Thermosphere extension of the Whole Atmosphere Community Climate Model. *Journal of Geophysical Research*, *115*(A12), A12302. https://doi.org/10.1029/2010JA015586

Marcos, F. A., Wise, J. O., Kendra, M. J., Grossbard, N. J., & Bowman, B. R. (2005). Detection of a long-term decrease in thermospheric neutral density. *Geophysical Research Letters*, *32*(4), L04103. https://doi.org/10.1029/2004GL021269

Mlynczak, M. G., Hunt, L. A., Mertens, C. J., Thomas Marshall, B., Russell, J. M., III, Woods, T., et al. (2014). Influence of solar variability on the infrared radiative cooling of the thermosphere from 2002 to 2014. *Geophysical Research Letters*, *41*(7), 2508–2513. https://doi.org/10.1002/2014GL059556

Nandy, D. (2021). Progress in solar cycle predictions: Sunspot cycles 24–25 in perspective: Invited review. *Solar Physics*, *296*(3), 54. https://doi.org/10.1007/s11207-021-01797-2

Picone, J. M., Hedin, A. E., Drob, D. P., & Aikin, A. C. (2002). NRLMSISE-00 empirical model of the atmosphere: Statistical comparisons and scientific issues. *Journal of Geophysical Research*, *107*(A12), 1468. https://doi.org/10.1029/2002JA009430

Qian, L., Roble, R. G., Solomon, S. C., & Kane, T. J. (2006). Calculated and observed climate change in the thermosphere, and a prediction for solar cycle 24. *Geophysical Research Letters*, *33*(23), L23705. https://doi.org/10.1029/2006GL027185

Qian, L., & Solomon, S. C. (2011). Thermospheric density: An overview of temporal and spatial variations. *Space Science Reviews*, *168*(1–4), 147–173. https://doi.org/10.1007/s11214-011-9810-z

Roble, R. G., & Dickinson, R. E. (1989). How will changes in carbon dioxide and methane modify the mean structure of the mesosphere and thermosphere? *Geophysical Research Letters*, *16*(12), 1441–1444. https://doi.org/10.1029/GL016i012p01441

Saunders, A., Lewis, H. G., & Swinerd, G. G. (2011). Further evidence of long-term thermospheric density change using a new method of satellite ballistic coefficient estimation. *Journal of Geophysical Research*, *116*(A2), A00H10. https://doi.org/10.1029/2010JA016358

Siemes, C., Borries, C., Bruinsma, S., Fernandez-Gomez, I., Hładczuk, N., den IJssel, J., et al. (2023). New thermosphere neutral mass density and crosswind datasets from CHAMP, GRACE, and GRACE-FO. *Journal of Space Weather and Space Climate*, *13*, 16. https://doi.org/10.1051/swsc/2023014

Solomon, S. C., Liu, H. L., Marsh, D. R., McInerney, J. M., Qian, L., & Vitt, F. M. (2018). Whole atmosphere simulation of anthropogenic climate change. *Geophysical Research Letters*, *45*(3), 1567–1576. https://doi.org/10.1002/2017GL076950

Solomon, S. C., Liu, H. L., Marsh, D. R., McInerney, J. M., Qian, L., & Vitt, F. M. (2019). Whole atmosphere climate change: Dependence on solar activity. *Journal of Geophysical Research: Space Physics*, *124*(5), 3799–3809. https://doi.org/10.1029/2019JA026678

Solomon, S. C., Qian, L., & Roble, R. G. (2015). New 3-D simulations of climate change in the thermosphere. *Journal of Geophysical Research: Space Physics*, *120*(3), 2183–2193. https://doi.org/10.1002/2014JA020886

Sutton, E. K., Thayer, J. P., Wang, W., Solomon, S. C., Liu, X., & Foster, B. T. (2015). A self-consistent model of helium in the thermosphere. *Journal of Geophysical Research A: Space Physics*, *120*(8), 6884–6900. https://doi.org/10.1002/2015JA021223

Walker, J. C. G. (1965). Analytic representation of upper atmosphere densities based on Jacchia's static diffusion models. *Journal of the Atmospheric Sciences*, *22*(4), 462–463. https://doi.org/10.1175/1520-0469(1965)022%3C0462:AROUAD%3E2.0.CO;2

Weng, L., Lei, J., Zhong, J., Dou, X., & Fang, H. (2020). A machine-learning approach to derive long-term trends of thermospheric density. *Geophysical Research Letters*, *47*(6), e2020GL087140. https://doi.org/10.1029/2020GL087140

Yue, J., Russell, J., III., Jian, Y., Rezac, L., Garcia, R., López-Puertas, M., & Mlynczak, M. G. (2015). Increasing carbon dioxide concentration in the upper atmosphere observed by SABER. *Geophysical Research Letters*, *42*(17), 7194–7199. https://doi.org/10.1002/2015GL064696